Journal of Thermal Engineering
Web page info: https://jten.yildiz.edu.tr
DOI: 10.18186/thermal.1117345

Research Article

CFD analysis andheat transfer characteristics of printed circuit heat exchanger

N. EL-HAKIM[1], J. ASSAF[1], B. NEHME[2], B. ZEGHONDY[3], W. SAID[1], J. JELWAN[3]*

[1]*Department of Chemical Engineering, Holy Spirit University of Kaslik (USEK), Jounieh, Lebanon*
[2]*Department of ETC Engineering, Holy Spirit University of Kaslik (USEK), Jounieh, Lebanon*
[3]*Department of Mechanical Engineering, Holy Spirit University of Kaslik (USEK), Jounieh, Lebanon*

ARTICLE INFO

Article history
Received: 18 August 2020
Accepted: 20 November 2020

Keywords:
PCHE; SCO_2; Cubical Fins; Enhance Heat Transfer; Fanning Friction Coefficient

ABSTRACT

This paper aims to investigate the cubical fins and the thermal-hydraulic characteristics in a Printed Circuit Heat Exchanger (PCHE). The working fluid is considered a supercritical LNG. The outcomes show that the thermal-hydraulic performance is enhanced using the cubical fins comparing it to the straight channel. The maximum and minimum difference of N_u/E_u between the cubical fins channel and the straight channel were 71.7% and 64.8% respectively. It is noticed that the pressure drop and Heat Transfer coefficient are increasedsimultaneously with increasing the mass flux.Using Ansys Fluent 15.0, numerical optimization isperformed to examine and analyzethe influence of the sparser staggered arrangement. The computed results show that this type of arrangement improves the thermal-hydraulic efficiency of the cubical fins in a PCHE. A comparison between the straight fins arrangement and the staggered fins arrangement is reported. It has been noticed that the velocity of the LNG flow in the cubical fins channel is increased along the length of the PCHE, and decreased byincreasing the vertical separation L_V. The side effect of the vertical separation L_V on the PCHE's efficiency was more evident than that of the staggered arrangement L_S. Finally, afeasibility study is performed to inspect the power consumption of the new design.

Cite this article as: El-Hakim N, Assaf J, Nehme B, Zeghondy B, Said W, Jelwan J. CFD analysis andheat transfer characteristics of printed circuit heat exchanger. J Ther Eng 2022;8(3):335–348.

INTRODUCTION

Designing a Printed Circuit Heat Exchanger (PCHE) has drawn considerable interest from designers and analysts. Multiple factual designstructural shape optimization of a heat exchanger using diverse replicas have been proposed by many researchers to find the geometry most favourable to simultaneously maximize heat exchanger temperature difference while costing a minimum pressure drop. For instance, Wakim et al. [1] investigate the plate-fin

***Corresponding author.**
*E-mail address: jadjelwan@usek.edu.lb

This paper was recommended for publication in revised form by Regional Editor Sergey Glazyrin

Published by Yıldız Technical University Press, İstanbul, Turkey

heat exchangers using computational fluid dynamics (CFD) and modeling a series of topology enhancements. His model is expressed by a user-defined function to optimize the porous medium having a sequenceof high and low porosity. Consequently, the 3D straight fin structure has been diverted and tested for a quick enhancement with constant heat flux. It has been observed that this approach resultsin a dropin fin weight anda pressure drop of 23% and 13% respectively while conserving the same heat enrichment. Embracing this technique for the FSRU heat exchanger is ultimate, andconstructivefeaturescould be exploited to improve the LNG process.

The most important component of the LNG process is the heat exchanger which vaporizes the liquefied natural gas using a specific heating medium such as seawater or other means. This transfer procedure implicates in power production as a direct and/or an indirect contact, where the mechanism of the Heat Transfer follows the geometry of the fins. For an FSRU heat exchanger, LNG is normally heated up using seawater. In such an application, heat exchangers are subject to corrosion due to high salinity water, imposing the plant to a finite life cycle. Relatively, a reduction of rate energy transfer is expected, resulting in an increase in fluid mixing and velocities andinitiating a decline of the fluid flow properties where the thermal conductivity and density are radicallydisoriented.

To conquer the corrosion problem, yet, acquire high energy efficiency, robust and more thermally-conductive materials are desired.Cohen et al. [2],conduct a parametric analysis of a highly thermal conductivity polymer. His application was based on a doubly finned heat exchanger. Cohen observed that heat exchangers made from polymers offer a promising alternative material in designing heat exchangers in seawater cooled comparing it to aluminum heat exchangers.Such heat exchangers offerbetter corrosion resistance. This observation is affirmed by Zaheedet al.[3],underpinning the prominent use of the polymer film heat exchanger and addressing the disadvantages of the metallic heat exchangers.

Although polymers arerecognized to be an effective physical material for thermal conductivity, most of the research which has been compiled from the literature was about the flexibility of the PCHE channels[4, 5]. For instance, Lee et.al[4]conducted a CFD analysis for a PCHE channel made of a thin plate for various thermal performances. Lee's.et. al [5]simulation was optimized with a variable Reynolds number of 67×10^3 to 280×10^3. He found out that reducing the space of Heat Conduction and expanding the overlapping area sandwiched betweenthe hot and cold channels will maximize the Heat Transfer rate. Kwon et.al[6]studied the thermal efficiency of the Printed Circuit Heat Exchanger using mini channels in various cryogenic heat transfer conditions. His experimental results show a percentage of error of 5% for Reynolds numbers ranging from 8500 to 17×10^3. This percentage of error is significantly increased by 20% once the Reynolds number is setup between the range of 2100 and 2500. Even though Kwon's work is distinctive and very substantial, the cryogenic application on the PCHE has been shown to obtain axial conduction causing a low thermal performance [7]. Most of the analyses and experiments which have been channeled on PCHE are engaged using helium and water [8, 9, 10]. For instance, Figleyet al. [8], tested a PCHE in a high-temperature helium facility and developed a mathematical model. The numerical model was associatedwith the geometric factors and material properties. The flow conditions were checked through a comparative along witha prognostic investigation to assess the thermal efficiency and the Heat Transfer Performance of the Printed Circuit Heat Exchanger using the cross, parallel, and counter-flow PCHEs. Kim et al.[9] examined the thermal-hydraulic performance of Alloy 800H Printed Circuit Heat Exchanger using the helium test loop under variable mass flow rates ranging from 40 – 100 *kg/h*, operating under a pressure of 1.5 *MPa* and 1.9 *MPa* and an inlet temperature ranging between 25°C – 550°C. Pra et al. [10] conduct asteady-state assessment of a PCHE and examined its thermal-hydraulic performance in ahelium test ringat a temperature of 510°C. It has been observed that the effectiveness of the PCHE was about 95%. Moreover, a transient assessment was realized to induce the total life cycles in the heat exchanger. The process was repeated 100 times under different temperatures and unconventional channel geometries. Praet al.[10] reported that no trace of fatigue and failure was observed, and the reduction of the high-pressure drop was investigated numerically by performing a direct shape optimization procedure.

While the abovesections highlightsome of the work done using helium and water, many other researchers yield different approaches in their investigation.For instance, Nikitin et al. [11]investigated experimentally the heat transfer characteristics and the pressure drop features of the PCHE using supercritical water and supercritical CO_2. The experiment was conducted at an inlet temperature of 280°C to 300°C and a pressure of 2.2 to 3.2 *MPa* respectively. An empirical correlation was achieved to calculate the local heat transfer coefficient and pressure drop factor as a function of the Reynolds number. Moreover, supercritical CO_2 (S-CO_2) was investigated by Jeon et al.[12] using a heterogeneous type of PCHE. The thermal performance was optimized using different channel sizes and spacing between the channels. Jeonet al.[12] reported that the thermal performance is very sensitive to the adjustment of spacing, and the results are affected significantly. However, it has been observed that the hydraulic diameter and the thermal performance remain constant by modifying the channel cross-section.Kim et al.[13] examined the heat transfer and pressure drop characteristics of supercritical CO_2 flow in a PCHE model that incorporates airfoil-shaped fins. A comparative study between airfoil fin and zigzag PCHE channel configurations showed a significant decrease in pressure

Table1: Different configurations for the cubical fins position

Configuration(s)	1	2	3	4	5	6	7	8	9
L_v (*mm*)	1.3	1.3	1.3	1.67	1.67	1.67	2	2	2
L_s (*mm*)	0	0.4	0.8	0	0.4	0.8	0	0.4	0.8
Width (*mm*)	3.9	3.9	3.9	5.01	5.01	5.01	6	6	6
L_h (*mm*)	1.2	1.2	1.2	1.2	1.2	1.2	1.2	1.2	1.2
Thickness (*mm*)	0.75	0.75	0.75	0.75	0.75	0.75	0.75	0.75	0.75

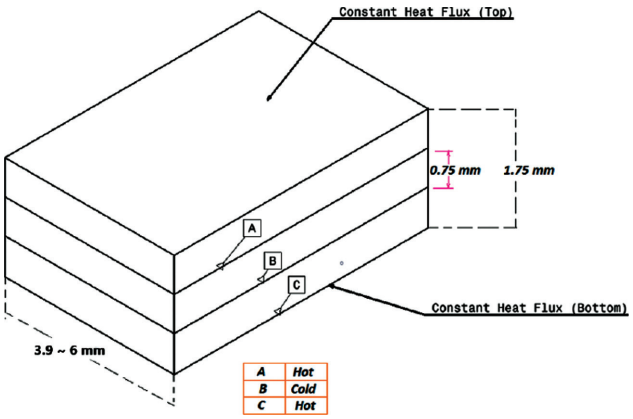

Figure 1: Complete configuration of the PCHE model.

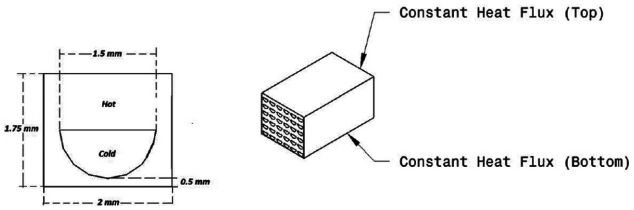

Figure 2: Fluid passage configuration with a semicircular cross flow.

drop. In a recent study by Zhao et al.[14], a new sort of microchannel PCHE heat exchanger is proposed. Sparser staggered airfoil fin arrangement has been investigated using the supercritical LNG as a working fluid. It has been reported that the thermal-hydraulic performance in airfoil fin PCHE is considerably improved.

In light of the above discussion, most of the proposed PCHE fin-type models are very complex to manufacture and require lots of optimization and predictive analysis to select the NACA number of the airfoil, each of which has its characteristics in terms of quantifying its mass and its energy saving. Hence, the objective of this paper is to thermally conduct a customary type of fin system within a heat exchanger made of steel materialand compare it to the results obtained by Zhao et al.[15],the details of which are represented in the following sections.

SYSTEM CONFIGURATION, MODELLING, AND SIMULATION ENVIRONMENT

Physical Model and Cube Fin Arrangement Parameters

In this paper, a cube-fin PCHE model was considered. Figures1 and 2showthe complete configuration of the PCHE model and the fluid passage configuration with a semicircular crossflow at entry and exit regions with a diameter of 1.5 mm. The heat exchanger is made of steel with thermal conductivity of 16.27 *W/*(*m.K*) as reported in [15]. The PCHE has a full length of 260 *mm*,1 cold and 2 hot plates diffusion bonded in a single banking pattern with 18 cubical fins. Figure 3shows the cube fins arrangements. For simplicity, 157 periodic cubic fin structures along one channel were selected with a total length of 260 *mm*. The staggered pitch L_s and the vertical pitch L_v were 0 *mm* and 1.67 *mm* respectively.CFD analysis has been carried out using 9 different configurations (refer to table 1 for more details) to acquire a comparative study between different fins arrangements. The flow characteristics and heat transfer of different cubicalfins configurations were investigatedusing six periodic fins (see figure 4 for more details) all along the streampath, and three in the oriented transverse direction. The same length and the same hydraulic diameter were employed for both states.From figure 3, L_h represents the split gap sandwiched between a cube top and adjacent cube top of the same string, and L_v represents the distance separating two vertical rows in the vertical direction. Accordingly, the width (W) varied from 3.9 to 6 mm (refer to figure 5 for more details). All configurations are tabulated in table 1.

Materials Properties And Boundary Conditions

The performance of any heat exchanger can be optimized by relating the total heat transfer rateq, heat transfer surface area A, the heat capacity of each fluid C_p, overall heat transfer coefficient U and fluid terminal temperatures. The fluid considered in these simulations is supercritical LNG, which thermo-physical properties are reported in [14, 15]. The applied boundary conditions in this paper were10MPa and 121K at the inlet, exceeding its critical pressure of P_{cr} = 4.59 MPa, with a mass flux of 325 kg/(m^2.s). The thermo-physical properties of the supercritical LNG are reported

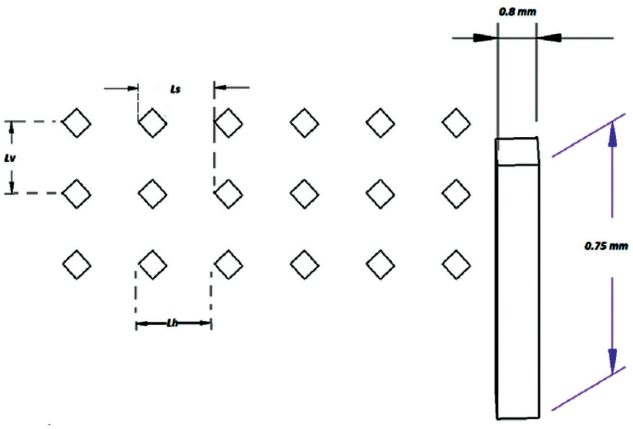

Figure 3: Cube fins arrangement and dimensions.

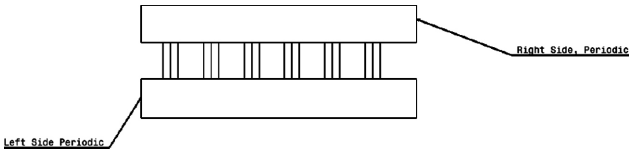

Figure 4: Section view of the cube fin channel.

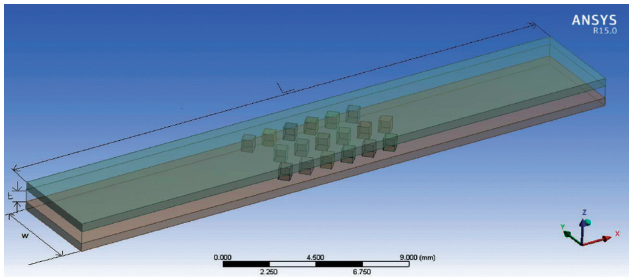

Figure 5: Configuration of one channel.

in [14]. For simplicity, the flow channel is prearranged as periodic in both transverse and longitudinal directionsas it is shown in Figure 4.

Supercritical LNG is used as the working fluid and steel is chosen as the material of construction for the plates and fins as well. The outlet boundary condition was defined by a pressure of 0 *Pa*. The heating medium used was seawater maintained at 298 *K* with the aid of exhaust fumes and BOG if it is lower than the desired temperature and a mass flow rate of 30 *kg/s*. Subsequently, the heat provided by the medium over the heat exchanger of 1 m^2 surface area is:

$$\dot{Q} = hA_s(T_\infty - T_s) \tag{1}$$

T_s is the surface temperature and it is considered 210 *K*. The properties of the steel plate are:

k = 0.60603 *W/m.K*, L = 1 *m*, whereas the properties of the seawater at a mean temperature of 298 *K* are ρ = 1035 Kg/m^3 for a salinity concentration of 0.035*g salt*/*g* water. This leads to dimensionless numbers Pr = 6.13, $\vartheta = 8.927 \times 10^{-6}$ m^2/s. The thickness of the water channel is 1 *mm*, and the width of 1m. Therefore, the cross-sectional area is equal to 0.001 m^2. Accordingly, the velocity is calculated as:

$$V = \frac{\dot{m}}{\rho \times A_C} \tag{2}$$

Hence, the Reynolds number is calculated as:

$$Re_L = \frac{V \times L}{\vartheta} \tag{3}$$

Consequently, the convective heat transfer h could be calculated using the following relation:

The Nusselt number is calculated as follows:

$$Nu = \frac{h \times L}{k} = 0.3387 \times Re_L^{\frac{1}{2}} \times Pr^{\frac{1}{3}} = 1116.97 \tag{4}$$

Using equations (2), (3), and (4), the velocity is computed as 28.99 *m/s*, Re_L = 3246948.27, Nu = 1116.97, h = 676.91 $W/m^2.K$. Thus, the rate of heat transfer per unit area is 58891 *W*. While the left and right walls are considered to be adiabatic, the top and bottom walls are predetermined with a constant heat flux of 58891 W/m^2 conducted throughout a thickness of 0.5 *mm*, and an outlet pressure was determined as 0 *Pa*.

Numerical Approach

ANSYS FLUENT R15.0[17] is used to solve the governing equations for 3D steady flow and heat transfer in the PCHE channel. The governing equations are represented as the following:

x – Momentum:

$$\frac{\partial}{\partial t}\rho u + \frac{\partial \rho u^2}{\partial x} + \frac{\partial \rho uv}{\partial y} + \frac{\partial \rho uw}{\partial z} + \nabla_{ij} = 0 \tag{5}$$

y – Momentum:

$$\frac{\partial}{\partial t}\rho v + \frac{\partial \rho uv}{\partial x} + \frac{\partial \rho v^2}{\partial y} + \frac{\partial \rho vw}{\partial z} + \nabla_{ij} = 0 \tag{6}$$

z – Momentum:

$$\frac{\partial}{\partial t}\rho w + \frac{\partial \rho uw}{\partial x} + \frac{\partial \rho vw}{\partial y} + \frac{\partial \rho w^2}{\partial z} + \nabla_{ij} = 0 \tag{7}$$

Conservation of Mass equation:

$$\frac{\partial u}{\partial x} + \frac{\partial v}{\partial y} + \frac{\partial w}{\partial z} = \frac{dP}{dt} \tag{8}$$

ρ is the density; u, v, w are the vector velocities; and P is the operating pressure.The k–ω model is substantially more used than k–ε[18].This model is good to describe the pressure gradient for any application [19]. The mathematical form of this model is:

$$\frac{\partial}{\partial t}(\rho k)+\frac{\partial}{\partial x_i}(\rho k u_i)+\frac{\partial}{\partial x_j}\left(T_k\frac{\partial k}{\partial x_j}\right)+G_w-Y_w+S_w \quad (9)$$

$$\frac{\partial}{\partial t}(\rho \omega)+\frac{\partial}{\partial x_i}(\rho \omega u_i)+\frac{\partial}{\partial x_j}\left(T_\omega\frac{\partial \omega}{\partial x_j}\right)+G_w-Y_w+S_w \quad (10)$$

The effective diffusivities for the k–ω model are given by:

$$T_k=\mu\frac{\mu_t}{\sigma_k} \quad (11)$$

$$T_\omega=\mu\frac{\mu_t}{\sigma_\omega} \quad (12)$$

From equation 12μ_t, is computed by combining k and ω as follows:

$$\mu_t=\alpha^*\frac{\rho k}{\omega} \quad (13)$$

The coefficient α^* damps the turbulent viscosity causing a low-Reynolds number correction. The SST model is formulated as the following:

$$\frac{\partial(\rho k)}{\partial t}+\frac{\partial(\rho U_i k)}{\partial x_i}=\tilde{P}_k-\beta^*\rho k\omega+\frac{\partial}{\partial x_i}\left[(\mu+\sigma_k\mu_t)\frac{\partial k}{\partial x_i}\right] \quad (14)$$

Equation (14) could be re-written in terms of a blending function denoted as:

$$\begin{aligned}&\frac{\partial(\rho\omega)}{\partial t}+\frac{\partial(\rho U_i\omega)}{\partial x_i}=\alpha\rho S^2-\beta\rho\omega^2\\&+\frac{\partial}{\partial x_i}\left[(\mu+\sigma_\omega\mu_t)\frac{\partial\omega}{\partial x_i}\right]+2(1-F_1)\rho\sigma_{\omega2}\frac{1}{\omega}\frac{\partial k}{\partial x_i}\frac{\partial\omega}{\partial x_i}\end{aligned} \quad (15)$$

S is the invariant strain rate and F_1 is expressed as:

$$F_1=tanh\left\{\left\{min\left[max\left(\frac{\sqrt{k}}{\beta^*\omega y'},\frac{500\upsilon}{y^2\omega}\right),\frac{4\rho\sigma_{\omega1}k}{CD_{k\omega}Y^2}\right]\right\}^4\right\} \quad (16)$$

$$CD_{k\omega}=max\left(2\rho\sigma_{\omega2}\frac{1}{\omega}\frac{\partial k}{\partial x_i}\frac{\partial\omega}{\partial x_i},10^{-10}\right) \quad (17)$$

$$\mu_t=\frac{a_1k}{\max(a_{1w},SF_2)} \quad (18)$$

$$F_2=tanh\left\{\left\{\left[max\left(\frac{2\sqrt{k}}{\beta^*\omega y'},\frac{500\upsilon}{y^2\omega}\right),\frac{4\rho\sigma_{\omega2}k}{CD_{k\omega}y^2}\right]\right\}^2\right\} \quad (19)$$

To prevent the build-up of turbulence in stagnation regions, a production limiter is introduced as:

$$P_k=\mu_t\frac{\partial U_i}{\partial x_j}\left(\frac{\partial U_i}{\partial x_j}+\frac{\partial U_j}{\partial x_i}\right),P_k=min(P_k,10.\beta^*\rho k\omega) \quad (20)$$

The constants of this model are computed by a blend function given as [18]:

$$\alpha=\alpha_1F+\alpha_2(1-F) \quad (21)$$

All constants of the k–ω, *SST* are tabulated in table 2.

The convective heat transfer coefficient is calculated using the equation below:

$$h=\frac{q_w}{T_w-T_{bulk}}=\frac{q_w}{T_w-(T_{in}+T_{out})/2} \quad (22)$$

Where q_w is the heat flux applied on the top and bottom wall, T_w is the area-averaged wall temperature. T_{in}, T_{out} and T_{bulk} are the inlet, outlet, and bulk temperature of LNG, respectively. The Nusselt number is calculated using the following equation:

$$Nu=\frac{hD_h}{\lambda} \quad (23)$$

With λ is the LNG thermal conductivity. The Reynolds number is calculated by:

$$Re=\frac{\nu\rho D_h}{\mu} \quad (24)$$

Table2: Shear Stress Transport Constants (Menter, 1991).

	$\sigma_{\omega1}$	$\sigma_{\omega2}$	β^*	β_1	β_2	α_1	α_2	σ_{k1}	σ_{k2}
SST	0.5	0.852	0.09	$\frac{3}{40}$	0.0828	$\frac{5}{9}$	0.44	0.85	1

Table 3: Hydraulic diameter calculation

	L_v =1.3 mm			L_v =1.67 mm			L_v = 2mm		
L_s(mm)	0	0.4	0.8	0	0.4	0.8	0	0.4	0.8
L(mm)	0.8	1.2	1.6	0.8	1.2	1.6	0.8	1.2	1.6
W(mm)	1.3	1.3	1.3	1.67	1.67	1.67	2	2	2
t(mm)	0.75	0.75	0.75	0.75	0.75	0.75	0.75	0.75	0.75
L_c(mm)	1.175	1.575	1.975	1.175	1.575	1.975	1.175	1.575	1.975
S_a(mm^2)	0.32	0.32	0.32	0.32	0.32	0.32	0.32	0.32	0.32
P_a(mm)	2.263	2.263	2.263	2.263	2.263	2.263	2.263	2.263	2.263
V(mm^3)	0.54	0.93	1.32	0.762	1.263	1.764	0.96	1.56	2.16
S(mm^2)	2.575	3.614	4.655	3.167	4.503	5.839	3.695	5.295	6.895
D_h(mm)	0.839	1.029	1.134	0.963	1.122	1.209	1.039	1.179	1.253

Where ρ and μ are the density and the dynamic viscosity of LNG, respectively. The total pressure drop between inlet and outlet is the sum of both friction and acceleration effect resulting from density augmentation.

$$\Delta P = \Delta P_{acc} + \Delta P_{fric} \tag{25}$$

$$\Delta P_{acc} = G^2\left(\frac{1}{\rho_{out}} - \frac{1}{\rho_{in}}\right) \tag{26}$$

$$\Delta P_{fric} = \frac{2 f L_u \rho v^2}{D_h} \tag{27}$$

Where ΔP is the total pressure drop between inlet and outlet. ΔP_{acc}, ΔP_{fric} are the acceleration and friction pressure drop, respectively. The wall shear stress is described as:

$$\tau_w = \mu \frac{\partial w}{\partial x} \tag{28}$$

This could be represented in terms of the mean velocity along the axial direction and the hydraulic diameter along the transverse direction as:

$$\tau_w \sim \mu \frac{u_m}{D_h} \tag{29}$$

Therefore, a relationship could be obtained between the Fanning friction factor and the wall shear stress as:

$$f = \frac{\tau_w}{\frac{1}{2}\rho u_m^2} \tag{30}$$

In this dimensionless study, the pressure loss coefficient is expressed in terms of the Euler number. It shows the relationship between dynamic velocity head, pressure drop, also the relative momentum loss rate, as follows:

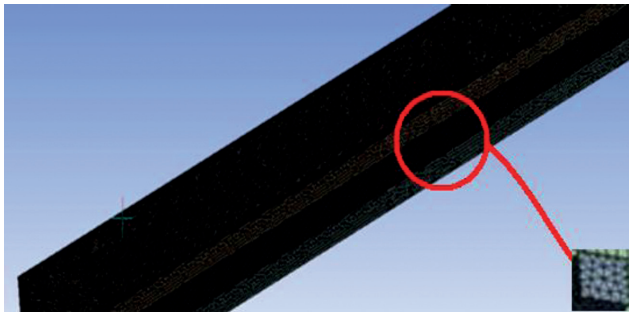

Figure 6: Mesh strategy.

$$E_u = \frac{\Delta P}{\frac{\rho u^2}{2}} \tag{31}$$

In a dimensionless study, it is necessary to determine the hydraulic diameter "D_h" which means the characteristics length of the flow channel. Thus, the cube fin placement is considered periodic, so the hydraulic diameter is calculated using the equations below:

$$V = (LW - S_a)t \tag{32}$$

$$S = 2\left(\frac{P_a t}{2}\right) + 2(L - L_C)t + 2(WL - S_a) \tag{33}$$

$$D_h = 4V/S \tag{34}$$

Where S_a and P_a are the top area and the wet perimeter of the fin respectively. V and S represent the volume and side surface area of the flow channel, respectively. Table 3 shows the calculated hydraulic diameter D_h for each configuration.

The accuracy of the results is interrelated to the mesh approach.The inflation method was predetermined by

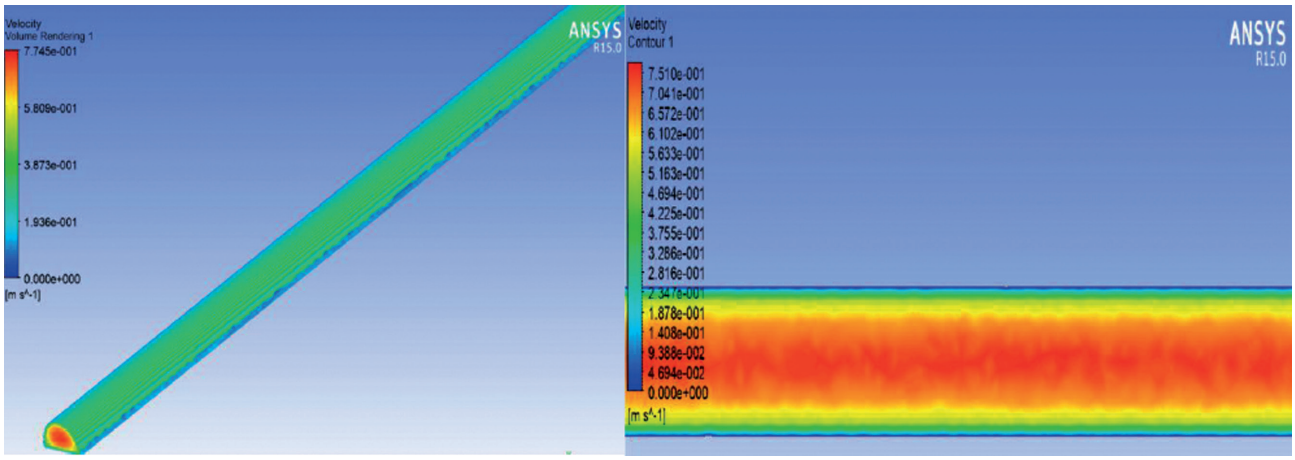

Figure 7: Straight channel velocity contour.

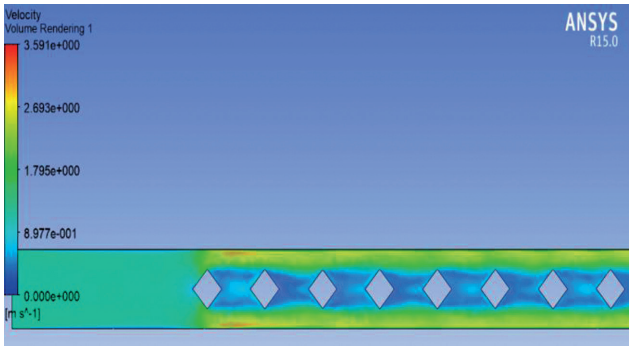

Figure 8: Cube fins channel velocity volume rendering.

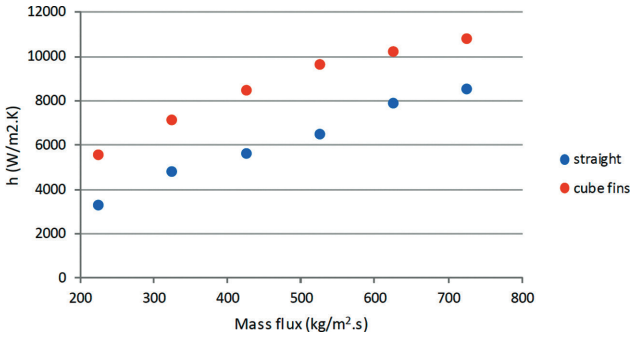

Figure 9: Heat transfer coefficient in the function of mass flux.

setting the thickness of the first boundary layer to 0.01 *mm* and setting six boundary layers near the bottom and top walls and fin surface described as sensitive areas for flow and heat transfer. The accuracy of the results is highly dependent on the grid density. Thus, an extremely fine grid of 3659194 elements was obtained with a mesh sizing of 0.09 *mm* (see figure 6). The residual for each parameter was set as 10^{-6}, and the second-order upwind was used.

RESULTS AND DISCUSSION

Comparison of Straight Channel Pche Vs Cube Fin PCHE

In this study, the flow characteristics of LNG and the heat transfer in the straight channel and cube fin PCHE were numerically investigated with the same hydraulic diameter (0.917 mm). Figure 7 shows the velocity contour in a straight channel and cube fin channel with a mass flux of 325 kg/m2.s.When the flow was continuously heated along the channel, the bulk velocity increaseddue to adropin its density. However, due to the continuous contraction and expansion in the sectional area of the channel, the velocity increases rapidly in the cube fins channel and reaches three times the velocity of the inlet at the contracted region of the cube fin. This could be explained that the cubical fins play a significant role in the LNG distribution causing a rise in the flow resistance and the heat transfer simultaneously, enhancing the distribution of the LNG from the outset of the cubical fins.

To investigate the effect of the mass flux, six different values were selected for a straight and cube fins PCHE respectively. Figures9 and10 display the heat transfer coefficient and the Nusselt number at various mass fluxes respectively. From figure 9, it is clearly shown that the turbulence intensity of the flow increases, this is due to a rise in the mass flux; thus, the heat transfer coefficient and Nusselt number are increased in both cases.

Referring to figure 10, the Nusselt number of the cube fins is higher than that of the straight channel. This could be explained by the fact that the flow and the heat transfer are highly affected by the fins in two different ways: the flow disturbance will increase and the heat transfer area will enlarge. Accordingly, the cube fin PCHE shows an improved thermal and hydraulic performance than that of

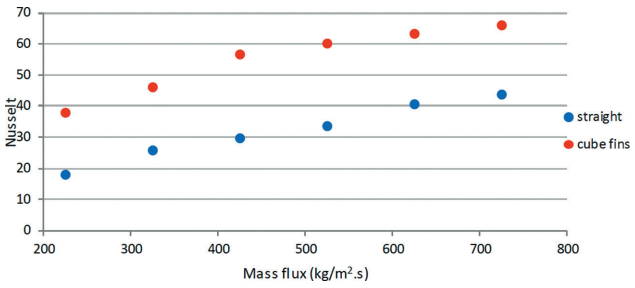

Figure 10: Nusselt number in the function of mass flux.

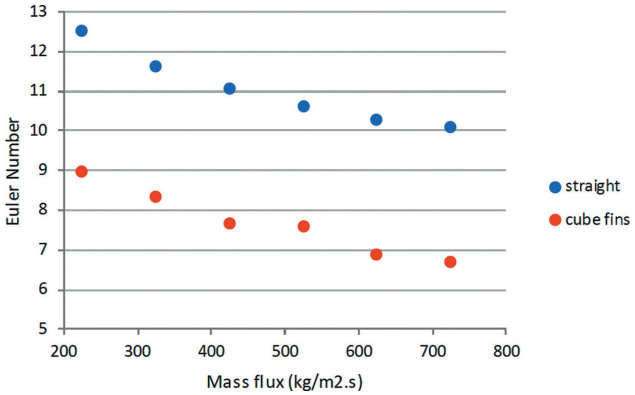

Figure 12: Euler number in the function of mass flux.

straight channel PCHE for the same hydraulic diameter and mass flux. As an example, for a mass flux G = 325 kg/m2.s and G = 725 kg/m2.s, the Nusselt values of cube fins PCHE were 2.36 and 1.89 times those of straight channels, respectively. To examine further the influence of mass flux, Euler number and Fanning friction factor are assessed. Figures 11 and 12 show the influence of mass flux on Euler number and the Fanning friction factor in both cases was also assessed. The Euler number of straight PCHE is depicted to be higher than that of cube fins. For instance, for a mass flux of 525 kg/m2.s, Euler number of cube fins was 71.3% of its value in the straight channel. As expected, the pressure drop is increased when the mass flux increases. Conversely, the Euler number decreasedwhen the mass flux increased. It is noteworthy thatthe Euler number is proportional to ΔP but inversely to V^2. Certainly, the velocity of the flow increases with increasing the mass flux leading to an increase in the pressure drop. Despite that, V^2 discharges an important effect on Euler rather than that of the pressure drop. As a result, the Euler number decreases for an increase in the mass flux.

The foremost indices of the heat transfer performance are designed by Nusselt and Euler number reciprocally. The optimal design was assessed by a specific option which is the ratio between Nusselt and Euler. Figure 13 shows the plot of N_u/E_u versus mass flux ṁ. The maximum and

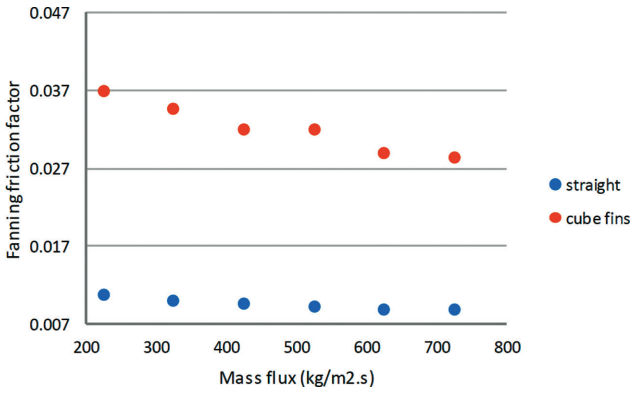

Figure 11: Fanning factor coefficient in the function of mass flux.

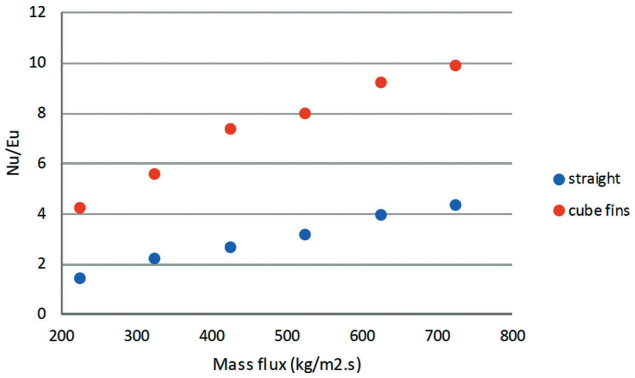

Figure 13: Plot of N_u/E_u in the function of mass flux.

minimum differences of the ratio between cube fin PCHE and straight channel PCHE were 51.07% and 46.2% subsequently. Noticeably, the cube fin PCHE represents an enriched thermal-hydraulic performance, and the ratio difference between cube fin and straight channel PCHEs increased withincreasing mass flux. Consequently, fin arrangement is favored for cube fin PCHE.

Staggered Pitch L_s Effect

Generally, the flow and heat characteristics were affected by the shape of the fins and their arrangement. In this study, the cube fins were first placed in parallel (L_s = 0 *mm*), and then in a staggered position (L_s = 0.4 and 0.8 *mm*) along the transverse direction.In cube fin PCHE, the fins have a narrow head and tail suitable for forming a smoother channel when the fins are staggered; also, it prevents the vortex separation due to the streamlined fins, leading to less flow resistance in a staggered position compared to that in a parallel arrangement. Figures 14, 15, and 16 describe the velocity contour of the flow in a cubefin PCHE positioned in parallel and staggered manners for a vertical pitch (L_v) of 1.3mm. At the inlet of the channels, the velocities of flow were relatively small and uniform

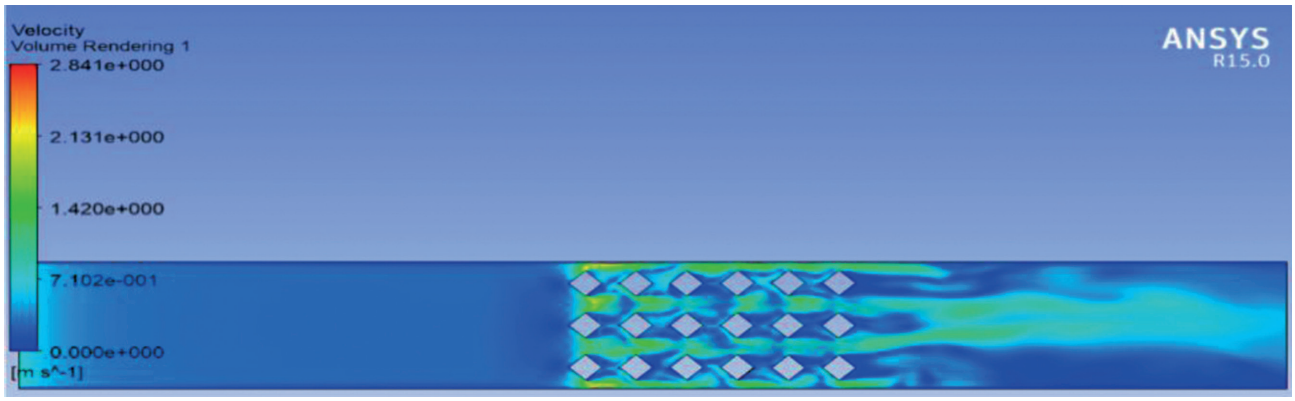

Figure 14: Velocity contour for L_v = 1.3 *mm* and L_s = 0 *mm*.

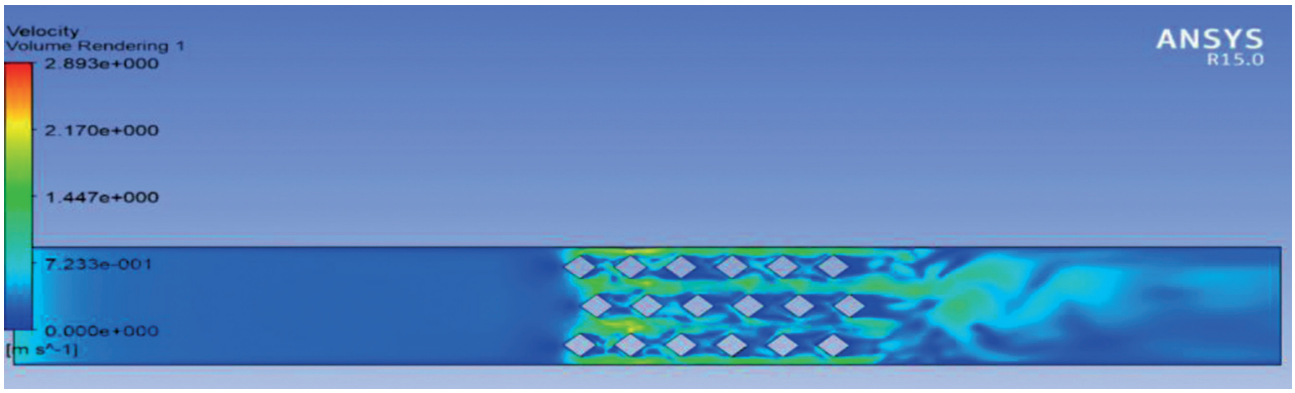

Figure 15: Velocity plot for L_v = 1.3 *mm* and L_s = 0.4 *mm*.

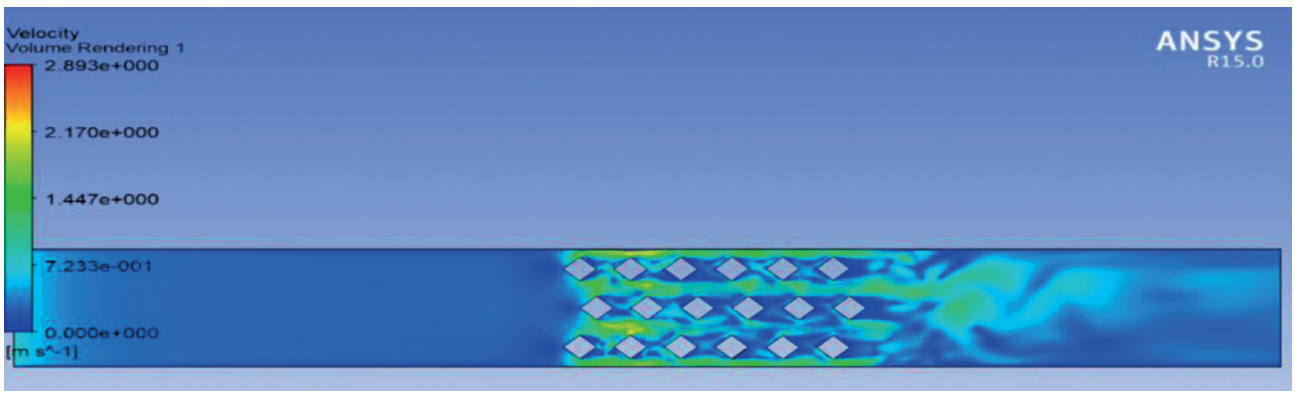

Figure 16: Velocity contour for L_v = 1.3 *mm* and L_s = 0.8 *mm*.

in both parallel and staggered arrangements. However, as a result of the continuous contraction and expansion of thesectional area of the flow channel, the velocity becomesuniform and it increased in the flow direction. Thus, the staggered arrangement promoted the formation designby creating a smooth flow channel and keeping the flow field more uniform.

Figure 17 displays the Nusselt number of a cube fin PCHE in parallel (L_s = 0 *mm*) and staggered positions (L_s = 0.4 *mm* and 0.8 *mm*). As expected, better thermal performance is revealed in the case of staggered arrangements. For instance, for L_v = 1.67 *mm*, the Nusselt number at L_s = 0 *mm* varies with that at L_s = 0.8 *mm* by 21.9%. Figure 20 shows the N_u/E_u the ratio in function of L_v. While increasing

the staggering number L_s, the ratio increased as well. As shown in figure 20, N_u/E_u has the lowest value at L_s = 0 *mm*, about 38% than that at L_s = 0.8 *mm*, indicating that L_s = 0.8 *mm* has better pressure drop and heat transfer. In general, staggered arrangement leads to less flow resistance and enhanced thermal-hydraulic performance. However, the pressure drop was more affected to L_s than heat transfer.

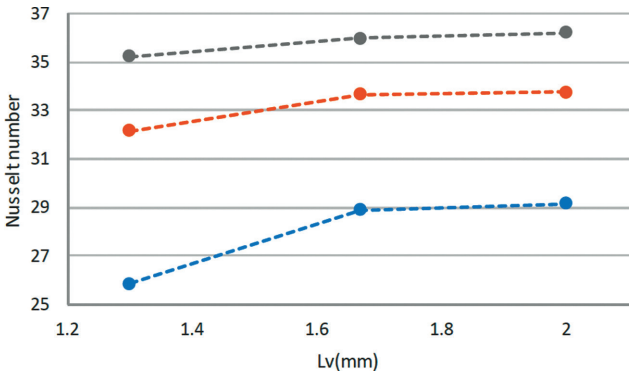

Figure 17: Plot of Nusselt number vs. L_v for different L_s.

Vertical Pitch (Lv) Effect

For constant L_h (1.2 *mm*), L_v directly specifies the width of the flow channel and the density of the fins. So, the consequence of changing L_v on the thermal and hydraulic performance of a cube, fin was analyzed.

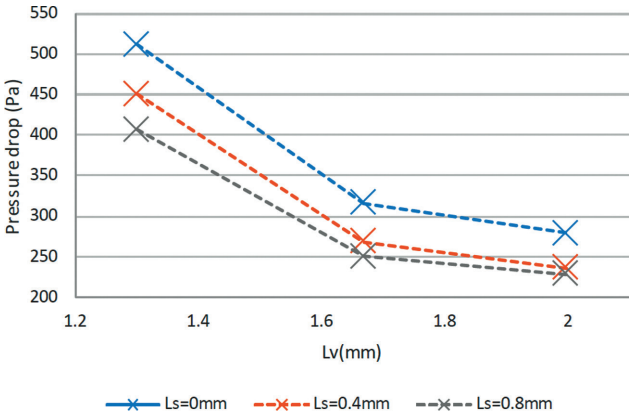

Figure 18: Plot of pressure drop vs. L_v at different L_s.

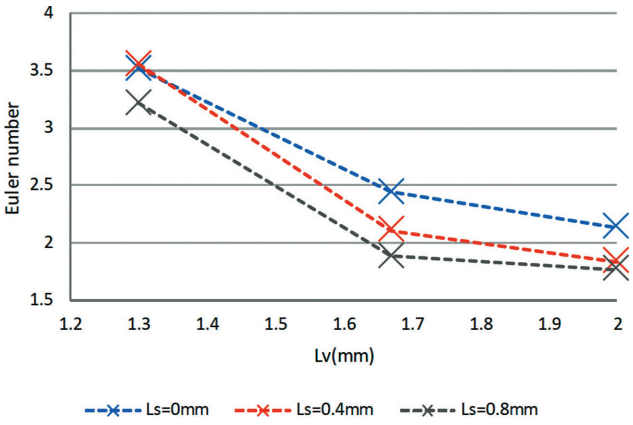

Figure 19: Plot of Euler number vs. L_v at different L_s.

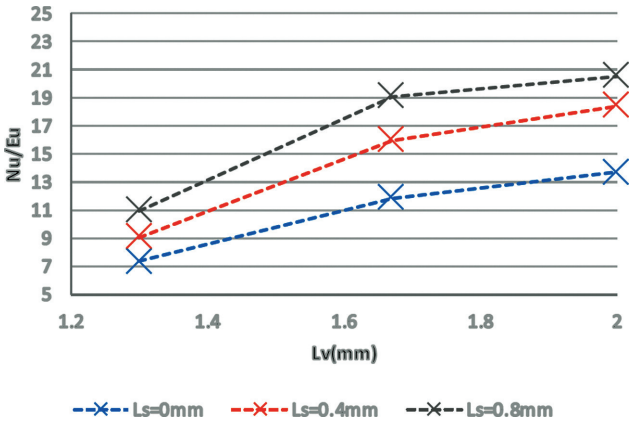

Figure 20: Plot of Nu/Eu vs. L_v at different L_s.

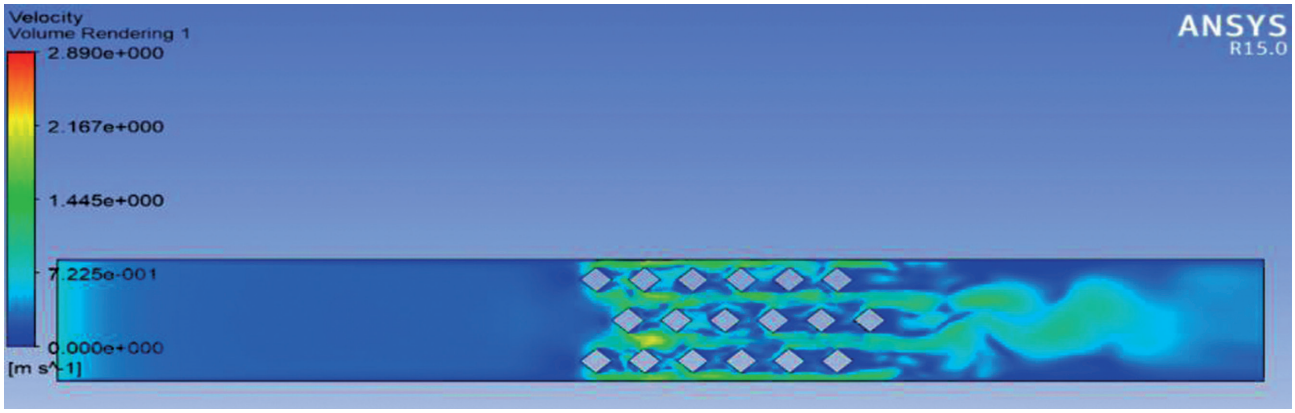

Figure 21: Velocity contour for L_v = 1.3 *mm* and L_s = 0.8 *mm*.

Figures 21-23 show the velocity contour of the flow in the cube fin PCHE disposed at different L_v while staggered at L_v = 0.8 *mm*. For a small vertical pitch L_v, the flow resistance is depicted to be higher, causing the flow velocity to increase. This is due to the narrow vertical separation L_v whichis controlled by athin flow channel sectional area. Accordingly, for the same inlet mass flux, the flow velocity increases with decreasing L_v. As an example, the maximum velocities of the flow in the adjoining sectional of the channel were about 0.91 m/s and 2.17 m/s with L_v = 2 *mm* and L_v = 1.3 *mm* respectively. Hence, the flow resistance and the turbulence intensity were both locally enhanced.

Figures 24 and 25 describe the variation of the heat transfer coefficient and Nusselt number in the function of L_v and at different L_s. Setting L_s unchanged, the convective heat transfer coefficient increased with decreasing L_v, which resultsin increased flow velocity. Figure 26 shows the effect of L_v on Euler number. The pressure drop decreased while increasing L_v. So for the same L_s, the Euler number dropped significantly with increasing L_v. For example, Euler number was about 54.8% at L_v = 2 *mm* comparing it to L_v = 1.3 *mm* for L_s = 0.8 *mm*. Therefore, reducing L_v improved the heat transfer but also result in an increased pressure drop.

As discussed previously, the ratio N_u/E_u was adopted to assess the efficiency of the cube fin PCHE (please refer to figure 27 for more details), N_u/E_u significantly increases as L_v rises. N_u/E_u at L_v = 2 *mm* is about 2 times and 1.16 times comparing it to L_v = 1.3 *mm* and L_v = 1.67 *mm* respectively, indicating that the condensed fin arrangement is optimal to enhance the heat transfer rate. At the same time, it is difficult to surpass flow resistance. Accordingly, the fins should be moderately arranged in the cube fin PCHE.

FEASIBILITY STUDY

A feasibility study is performed to investigate the power consumption of the new design. Accordingly, the pump power is emphasized and correlated to the pressure drop. It should be noted that for an incompressible fluid with a mass flow rate of $\dot{m}$, the power required by an adiabatic pump is defined as:

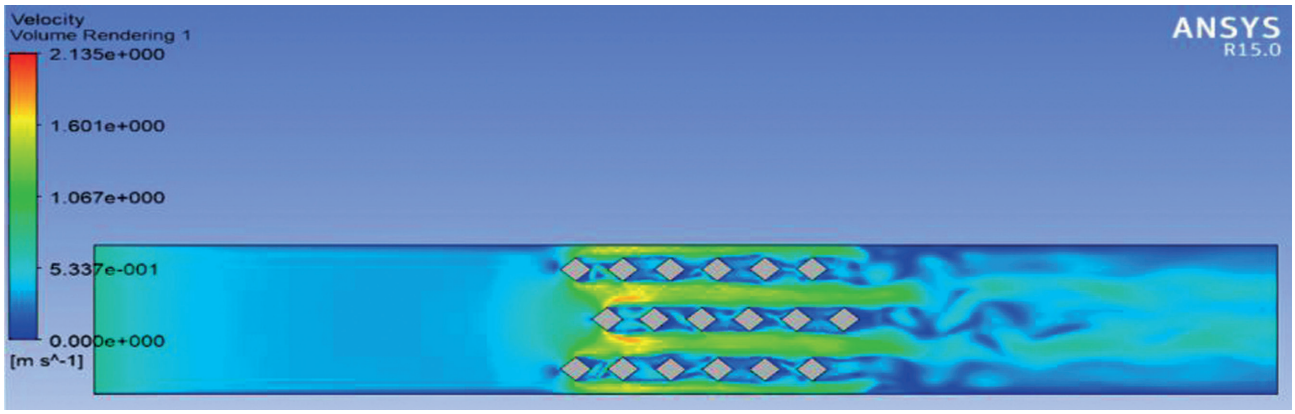

Figure 22: Velocity contour plot for L_v = 1.67 *mm* and L_s = 0.8 *mm*.

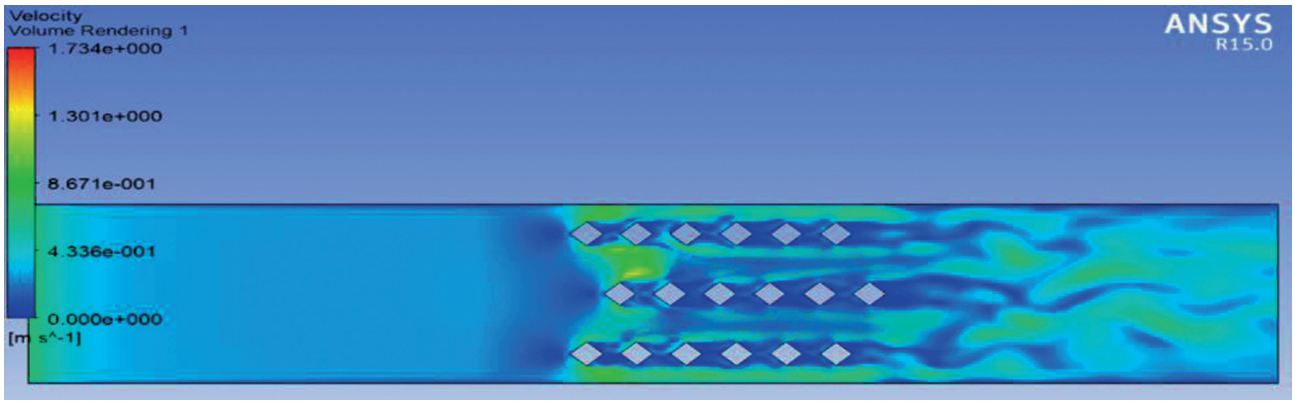

Figure 23: Velocity contour plot for L_v = 2 *mm* and L_s = 0.8 *mm*.

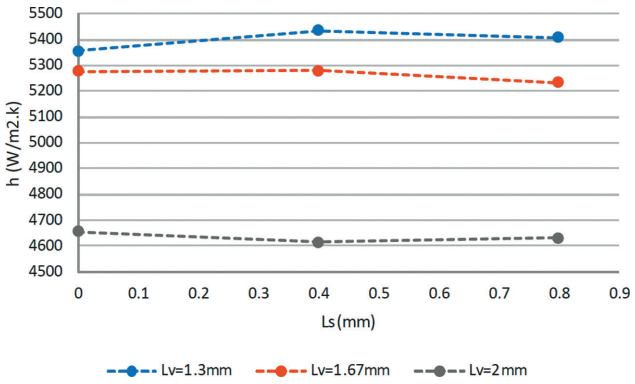

Figure 24: Heat transfer coefficient vs. L_s for different L_v.

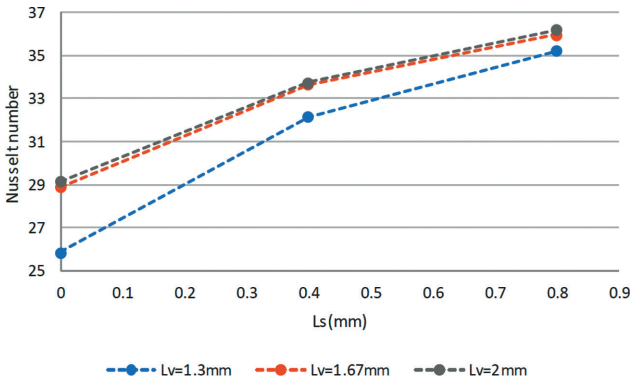

Figure 25: Nusselt number vs. L_s for different L_v.

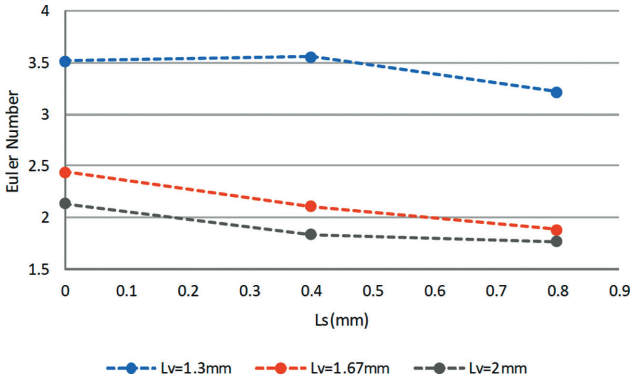

Figure 26: Euler number vs. L_s for different L_v.

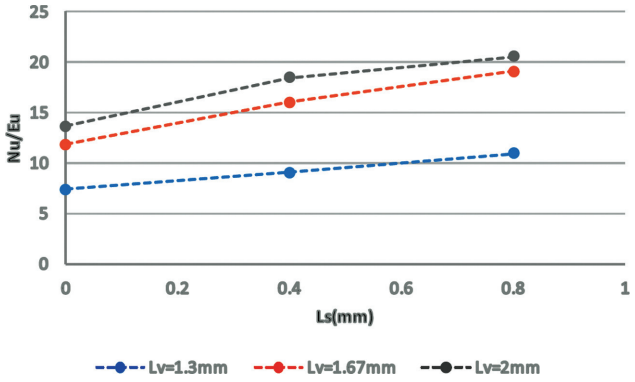

Figure 27: N_u/E_u vs. L_s for different L_v.

$$W_p = \frac{1}{\eta_p}\frac{\dot{m}}{\rho}\Delta p \tag{35}$$

Table 4 represents the parameters used to compute the power consumption in terms of USD.

Accordingly, table 5 represents a summary of the obtained results. It is clearly shown that once L_s increase the pressure drop decrease. This observation has been predicted for L_v as well, where the pressure drop decrease as L_v increases. Thus, this trend is strictly proportional to the power consumed by the pump, this has been observed in figure 28.

From figure 28, one can predict the cost-effectiveness of the fin arrangements. For L_v = 1.3 *mm*, for a variable L_s, it can be seen that the cost is extremely high with an optimum result for the heat transfer coefficient rates which enhance a better heat transfer rate. This value starts to decrease gradually for L_v = 1.67 *mm*, depicting a value of $h = 5277\frac{W}{m^2K}$, indicating a lower cost for comparing it to L_v = 1.3 *mm*. Thus, for L_v = 1.3 *mm*, it is clearly shown that the *h* is most of the time constant between L_s = 0 and L_s = 0.4 *mm*, corresponding to the lowest cost which is equivalent to 0.0018 USD at L_s = 0.4 *mm*. It should be noted that this value could be marginal since the lowest point is represented at L_v = 1.67 *mm* and L_s = 0.8 *mm*. However, for this particular case *h* has been perceived to decline, which is not the case of an efficient and well-enriched system performance. Finally, the predicted values for L_v = 2 *mm* is depicted to have the lowest heat transfer coefficient in all cases. Hence, this value is not considered any design point. It should be noted that this cost study, has been performed with a singlechannel within one plate. This study has been performed on 18 fins (6 in the longitudinal direction and 3

Table 4: Parameters to simulate the cost

KWh ($)	0.091
Mass flux (kg/m2.s)	325
Density (kg/m3)	447
Pump efficiency	0.9
Time (hr)	24

Table 5: Heat transfer coefficient and pumping cost calculation

Ac (m2)	0.000002925			3.7575E-06			0.0000045		
mass flow rate (kg/s)	0.000950625			0.001221188			0.0014625		
Lv(mm)	1.3			1.67			2		
Ls(mm)	0	0.4	0.8	0	0.4	0.8	0	0.4	0.8
ΔP(Pa)	511.665	450.348	406.522	315.862	268.47	249.994	278.659	236.332	227.962
Pump power (KW)	0.00120	0.00105	0.00095	0.00095	0.00081	0.00075	0.00100	0.00085	0.00082
Kwh consumed (KWh)	0.02882	0.02537	0.02290	0.022858	0.01942	0.01809	0.02415	0.02048	0.01975
h (w/m2.k)	5355.44	5435.29	5406.40	5276.9	5279.54	5231.55	4835.70	4939.59	4979.89
Cost ($)	0.00262	0.00230	0.00208	0.00208	0.00176	0.00164	0.00219	0.00186	0.0017

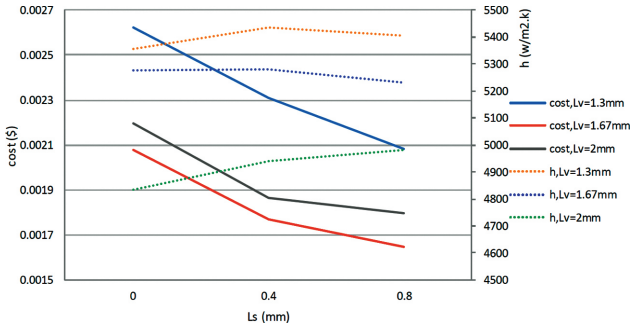

Figure 28: Plot of pumping cost and heat transfer coefficient for different configurations.

in the transverse direction), with periodic boundary conditions on the left and right hand of the channel as well as for the top and bottom.

To sum up, the relatively highest heat transfer coefficient that corresponds to the lowest pumping cost is achieved for L_v = 1.67 mm and L_s = 0.4 mm. This configuration corresponds to the optimal design of the PCHE.

CONCLUSION AND DESIGN OUTCOMES

This paper investigated the cubical fins in a PCHE and the thermal-hydraulic characteristics considering the working fluid as a supercritical LNG. It has been shown that the turbulence model *SSTK-ω* predicts very well the temperatures and the pressure drop. The obtained results show that the cube fins improved the thermal-hydraulic performance comparing it to the straight channel using LNG as a working medium. The maximum and minimum difference of Nu/Eu between the cube fin channel and the straight channel was 71.7 % and 64.8 % respectively. The pressure drop and heat transfer coefficient were raised in both PCHEs with increasing mass flux. Comparing the straight fin arrangements to the staggered fin arrangement, it is clearly shown that better thermal-hydraulic performance is acquired than the parallel arrangement. This has been observed for the same Lh and Lv, the cube fins arranged at Ls = 0.8mm presented a better thermal-hydraulic performance than those situated at other Ls. The velocity of LNG flow in the cube fin channel increased along the length and decreased with increasing Lv. The effect of vertical separation Lv on the PCHE's performance was more evident than that of staggered arrangement Ls. Regarding the analysis of the pressure drop and the heat transfer coefficient, the sparser staggered arrangement can enhance the thermal-hydraulic performance of the cube fin PCHE.

AUTHORSHIP CONTRIBUTIONS

Authors equally contributed to this work.

DATA AVAILABILITY STATEMENT

The authors confirm that the data that supports the findings of this study are available within the article. Raw data that support the finding of this study are available from the corresponding author, upon reasonable request.

CONFLICT OF INTEREST

The author declared no potential conflicts of interest with respect to the research, authorship, and/or publication of this article.

ETHICS

There are no ethical issues with the publication of this manuscript.

REFERENCES:

[1] Wakim S, Nemer M, Zeghondy B, Ghannam B, Bouallou C. Topology enhancement of plate and fin heat exchangers using a discrete porous media simulation approach, 4th Thermal and Fluids Engineering Conference, 14-17 April, Las Vegas, NV, USA, 2019. [CrossRef]

[2] Bar-Cohen A, Rodgers P, Cevallos J. Application of Thermally Conductive Thermoplastics to Seawater-cooled Liquid-Liquid Heat Exchangers, in Fifth European Thermal-Sciences Conference, Eindhoven, The Netherlands, 2008.

[3] Zaheed L, Jachuck RJJ. Review of polymer compact heat exchangers, with special emphasis on a polymer film unit. Appl Therm Eng 2004;24:2323–2358. [CrossRef]

[4] Lee SM, Kim KY. Optimization of zigzag flow channels of a printed circuit heat exchanger for nuclear power plant application. J Nucl Sci Technol 2012;49:343–351. [CrossRef]

[5] Lee, SY, Park BG, Chung JT. Numerical studies on thermal hydraulic performance of zigzag-type printed circuit heat exchanger with inserted straight channels. Appl Therm Eng 2017;123:1434–1443. [CrossRef]

[6] Dohoon K, Lingxue J, WooSeok J, Sangkwon J. Experimental investigation of heat transfer coefficient of mini-channel PCHE (printed circuit heat exchanger). Cryogenics 2018;92:41–49. [CrossRef]

[7] Baek S, Kim JH, Jeong S, Jung J. Development of highly effective cryogenic printed circuit heat exchanger (PCHE) with low axial conduction. Cryogenics 2012;52:366–374. [CrossRef]

[8] Figley J, Sun X, Mylavarapu SK, Hajek B. Numerical study on thermal hydraulic performance of a Printed Circuit Heat Exchanger. Prog Nucl Energy 2013;68:89–96. [CrossRef]

[9] Kim W, Baik YJ, Jeon S, Jeon D, Byon C. A mathematical correlation for predicting the thermal performance of cross, parallel, and counterflow PCHEs. Int J Heat Mass Transf 2017;106:1294–13022. [CrossRef]

[10] Pra F, Tochon P, Mauget C, Fokkens J, Willemsen, S. Promising designs of compact heat exchangers for modular HTRs using the brayton cycle. Nucl Eng Des 2008;238:3160–3173. [CrossRef]

[11] Nikitin K, Kato Y, Ngo L. Printed circuit heat exchanger thermal-hydraulic performance in supercritical CO2 experimental loop. Int J Refrig 2006;29:807–814. [CrossRef]

[12] Jeon S, Baik YJ, Byon C, Kim W. Thermal performance of heterogeneous PCHE for supercritical CO2 energy cycle. Int J Heat Mass Transf 2016;102:867–876. [CrossRef]

[13] Kim DE, Kim MH, Cha JE, Kim SO. Numerical investigation of thermal-hydraulic performance of new printed circuit heat exchanger model. Nucl Eng Des 2008;238:3269–3276. [CrossRef]

[14] Zhao Z, Zhao K, Jia D, Jiang P, Shen R. Numerical investigation on the flow and heat transfer characteristics of supercritical liquefied natural gas in an airfoil fin printed circuit heat exchanger. Energies 2017;10:1828. [CrossRef]

[15] Zhao Z, Zhou Y, Xiaolong M, Chen X, Li S, Yang S. Numerical study on thermal hydraulic performance of Supercritical LNG in Zigzag-Type Channel PCHEs. Energies 2019;12:548. [CrossRef]

[16] Higashi Y. NIST thermodynamic and transport properties of refrigerants and refrigerant matures (REFPROP). NetsuBussei 2000;14:1575–1577.

[17] ANSYS® Academic Research Mechanical, Release 15.0, 2013

[18] Menter FR. Influence of freestream values on k-omega turbulence model predictions, AIAA J 1991;30:1657. [CrossRef]

[19] Costa Rocha PA, Barbosa Rocha HH, Moura Carneiro FO, Vieira da Silva ME, Freitas de Andrade C. A case study on the calibration of the k–ω SST (shear stress transport) turbulence model for small scale wind turbines designed with cambered and symmetrical airfoils. Energy 2016;97:144-150. [CrossRef]